Performance evaluation of a membrane-based flat-plate heat and mass exchanger used for liquid desiccant regeneration

Hongyu Bai, Jie Zhu*, Ziwei Chen, Junze Chu, Yiwen Liu

Department of Architecture and Built Environment, the University of Nottingham, University Park, Nottingham, NG7 2RD, UK

Abstract

Liquid desiccant dehumidification system has gained much progress recently for its considerable energy saving potential without liquid water condensation. Within the system, regeneration is of great importance since diluted desiccant solution after dehumidification needs to be re-concentrated. The operational characteristics of a membrane-based flat-plate heat and mass exchanger used for liquid desiccant regeneration are investigated in this study. The liquid desiccant and air are in a cross-flow arrangement, and separated by semi-permeable membranes to avoid carry-over problem. The regeneration performance is examined by numerical simulation and experimental test. Solution side effectiveness, temperature decrease rate (TDR) and moisture flux rate (MFR) are applied to evaluate heat and mass transfer in the regenerator. Effects of main operating parameters are assessed, which include dimensionless parameters (i.e. number of heat transfer units NTU and solution to air mass flow rate ratio m^*), solution inlet properties (i.e. temperature $T_{sol,in}$ and concentration $C_{sol,in}$) and air inlet conditions (i.e. temperature $T_{air,in}$ and humidity ratio $W_{air,in}$). It is found that m^* and NTU are two of the most important parameters and their effects on the regeneration performance are interacted with each other. There is hardly benefit to the performance improvement by increasing NTU at low m^* or increasing m^* at low NTU. Even though the regeneration performance can be improved by increasing m^* and NTU, its improvement gradient is limited when m^* and NTU exceed 2 and 4 respectively. It is also found that increasing solution inlet temperature is an effective approach to enhance the regeneration performance, while air inlet temperature and humidity ratio have negligible effects on it.

Keywords: liquid desiccant, regeneration, numerical modelling, membrane-based flat-plate exchanger

* *Corresponding author. Tel: +44 1158466141. E-mail address: jie.zhu@nottingham.ac.uk*

Nomenclature

A	membrane surface area (m^2)
c_p	specific heat capacity (J/kgK)
C	concentration (%)
${C_r}^*$	thermal capacity ratio
d	width of the rectangular channel (m)
D	diffusivity (m^2/s)
h	convective heat transfer coefficient ($\mathrm{W/m^2K}$)
h_{fg}	condensation heat of water (J/kg)
h^*	operating factor
H	height of the dehumidifier unit (m)
k	thermal conductivity (W/m K)
L	length of the dehumidifier unit (m)
m^*	solution to air mass flow rate ratio
$\dot{m}$	mass flow rate (kg/s)
MFR	moisture flux rate
MRR	moisture removal rate (kg/s)
NTU	number of heat transfer units
NTU_m	number of mass transfer units
P	atmospheric pressure (pa)
P_v	equilibrium vapour pressure of desiccant solution (pa)
Re	Reynolds number
RH	relative humidity (%)
T	temperature (℃)
TDR	temperature decrease rate
U	overall heat transfer coefficient ($\mathrm{W/m^2K}$)
U_m	overall mass transfer coefficient ($\mathrm{kg/m^2s}$)
$\dot{V}$	volumetric flow rate (l/min)
W	humidity ratio ($kg/kg\ \ dry\ air$)
X	solution mass fraction

Greeks

ε	effectiveness
δ	thickness of membrane (m)
ρ	density ($\mathrm{kg/m^3}$)

Superscripts

$*$	dimensionless

Subscripts

air	air side
$crit$	critical value
$desi$	desiccant
exp	experimental
in	inlet
lat	latent
m	mass transfer
mem	membrane
num	numerical
out	outlet
sen	sensible
sol	solution side
tol	total

1. Introduction

Energy consumption by heating, ventilation and air-conditioning (HVAC) systems accounts for around 50% of the total energy consumed in buildings. A great portion of the energy consumption is associated with air dehumidification which is traditionally achieved by cooling the air below its dew point to reduce its moisture content in the cooling coil system. As a consequence, this leads to wet cooling coil surface that may cause growth of mould and bacteria, which result in undesirable healthy issues and poor indoor air quality. In addition, the overcooled air needs to be reheated to an appropriate temperature before supplied to the conditioned space, which leads to the consumption of additional energy [1-5].

In recent years, a great deal of attention has been devoted to liquid desiccant dehumidification systems, in which dehumidification is achieved by using liquid desiccant to absorb water vapour from moisture air directly. These systems have been proved to be more energy efficient, healthily and environmentally friendly than the conventional systems [6-8]. Packed-bed columns have been used for air dehumidification traditionally, in such a system air and desiccant solution are in direct contract, and small corrosive desiccant droplets are carried over by the processed air, which brings hidden concern to indoor environment and occupants [9, 10]. As a solution, semi-permeable membranes are applied as alternative heat and mass transfer media to solve desiccant carryover problem, air and desiccant are separated by the membranes in such a system. Furthermore, other harmful gases are also prevented from permeating to the air side through the membranes.

Many researches on the membrane-based liquid desiccant dehumidification have been conducted. Moghaddam et al. [11, 12] experimentally and numerically evaluated the performance of a counter-flow liquid-to-air membrane energy exchanger (LAMEE), and focused on the effects of thermal capacity ratio (Cr^*), heat and mass transfer direction and desiccant solution. They found that all effectiveness increase with Cr^* under all test conditions, and changing the solution concentration is one effective way to control the supply air humidity ratio. Moghaddam et al. [13] further tested a small-scale single-panel LAMEE under different air conditions, and discovered that the number of heat transfer units (NTU) has the most remarkable impact on the system effectiveness which always increases with NTU. Bai et al. [14] analysed the performance of a cross flow parallel-plate membrane-based dehumidifier experimentally and numerically by considering comprehensive operating parameters. They indicated that NTU and solution to air mass flow rate ratio (m^*) are two of the most important parameters. Zhang at al. [15, 16] studied heat and mass transfer in an air-to-air membrane based enthalpy exchanger under naturally formed boundary conditions rather than uniform temperature (concentration) and heat flux (mass flux) boundary conditions, and extended their work to solution-to-air membrane based enthalpy exchanger for liquid desiccant air dehumidification, then obtained the fundamental data such as Nusselt number and Sherwood number by solving conjugate heat and mass transfer equations directly [17, 18]. Huang et al. [19, 20] investigated internally-cooled parallel-plate membrane contractors with cross-flow and quasi-counter flow configurations, and found that the contractor effectiveness can be significantly improved compared to adiabatic one's. Qiu et al. [21] proposed an internally-cooled hexagonal parallel-plate membrane contractor (IHPMC), and calculated the laminar flow and heat transfer in IHPMC, which are useful for the performance evaluation, structure design of membrane contractors formed by IHPMC. Applications of membrane-based liquid desiccant humidification in real industry have also been reported [22-24].

The above researches [11-24] mainly focus on the dehumidification process. However, within the liquid desiccant dehumidification system, regeneration process is considered to be one of the most crucial processes since the diluted desiccant solution after dehumidification needs to be re-concentrated to realize the solution recycle [10]. Some studies have been carried out regarding regeneration. For instance, Fumo and Goswami [25], and Longo and Gasparella [26] studied the regeneration performances of counter-flow packed bed towers through experimental tests and mathematical simulations. Liu et al. [27] investigated the operating characteristics of a cross-flow direct contact regenerator based on experimental data. Li et al. [28] conducted a research into single-stage and double-stage photovoltaic driven regeneration systems, while Yang et al. [29] analysed the performance of a novel ultrasonic atomization liquid desiccant regeneration system. However, the above researches [25-29] deal with direct contact regeneration between the desiccant solution and air. Ge et al. [30] experimentally studied heat and mass transfer of a LAMEE used for solution regeneration, where the performance is evaluated by applying air side effectiveness. Moghaddam et al. [31] used solution side effectiveness to assess the performances of a LAMEE used as dehumidifier and regenerator by considering the influence of solution flow rate. The main objective of this paper is to investigate the effects of main operating parameters, such as dimensionless parameters (i.e. NTU and m^*), solution inlet properties (i.e. temperature $T_{sol,in}$ and concentration $C_{sol,in}$) and air inlet conditions (i.e. temperature $T_{air,in}$ and humidity ratio $W_{air,in}$) on the performance of a membrane-based heat and mass exchanger used for desiccant regeneration by numerical simulation and experimental test. Solution-side effectiveness, together with another two indicators: solution side temperature decrease rate (TDR) and moisture flux rate (MFR) are applied to evaluate the regeneration performance. This paper presents a comprehensive parametric analysis on membrane-based liquid desiccant regenerator, and provides valuable data for the development and operation of liquid desiccant dehumidification air-conditioning system.

2. Mathematical model

2.1. Governing equations

The structure of a membrane-based parallel-plate regenerator is depicted in Fig. 1(a). The air and solution channels are seperated by semi-permeable membranes, thus heat and vapour can be transferred through membranes while the desiccant solution is prevented from going through them. The coordinate system used in numerical modelling is given in Fig. 1(b). One air channel and one neighbouring solution channel are selected as the calculating domain.

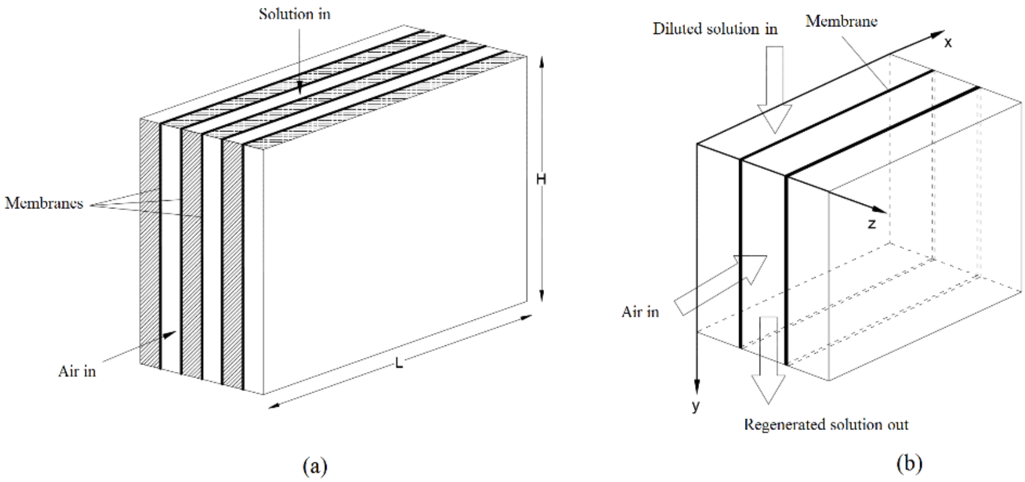

Fig. 1. (a) Structure of membrane-based parallel-plate regenerator, and (b) coordinate system used for numerical modelling.

Assumptions made for the sake of simplification in numerical modelling includes: well-insulated regenerator assumption; heat and mass transfer normal to the membrane; neglected heat conductions in air and solution channels; laminar flow assumptions in air and solution channels et al. More detailed assumptions can be found in authors' earlier work [14]. Compared to the dehumidifier, the directions of heat and mass transfer are conversed in the regenerator. Evaporative heat is taken from the solution side only since the solution side mass transfer coefficient is much higher than that in the air side. Then the governing equations for heat and mass transfer are given as:

Solution side:

$$\left(\frac{\dot{m}_{sol}}{L}\cdot\frac{\partial T_{sol}}{\partial y}\cdot C_{p,sol}\right)\cdot dxdy = -\left[U(T_{sol}-T_{air}) + h_{fg}\cdot U_m\left(W_{sol,mem}-W_{air}\right)\right]dxdy \quad (1)$$

$$\frac{\dot{m}_{desi}}{L}\cdot\frac{\partial X_{sol}}{\partial y}\cdot dxdy = -U_m\cdot\left(W_{sol,mem}-W_{air}\right)dxdy \quad (2)$$

Air side:

$$\left(\frac{\dot{m}_{air}}{H}\cdot C_{p,air}\cdot\frac{\partial T_{air}}{\partial x}\right)\cdot dxdy = U(T_{sol}-T_{air})dxdy \quad (3)$$

$$\left(\frac{\dot{m}_{air}}{H}\cdot\frac{\partial W_{air}}{\partial x}\right)\cdot dxdy = U_m\left(W_{sol,mem}-W_{air}\right)dxdy \quad (4)$$

Where L and H are length and height of regenerator (m) respectively, as illustrated in Fig. 1(a); $\dot{m}_{sol}$ is solution mass flow rate (kg/s); $\dot{m}_{desi}$ is desiccant mass flow rate (kg/s); $\dot{m}_{air}$ is air flow rate (kg/s); h_{fg} is water condensation heat (J/kg); T_{sol} is solution temperature (°C); T_{air} is air temperature (°C); W_{air} is air humidity ratio ($kg/kg\ dry\ air$); $W_{sol,men}$ is humidity ratio of membrane surface on solution side ($kg/kg\ \ dry\ air$); X_{sol} is solution mass fraction, which is calculated as:

$$X_{sol} = \frac{\dot{m}_{water}}{\dot{m}_{desi}} = \frac{1-C_{sol}}{C_{sol}} \quad (5)$$

Where C_{sol} is solution mass concentration:

$$C_{sol} = \frac{\dot{m}_{desi}}{\dot{m}_{sol}} \quad (6)$$

$C_{p,sol}$ is solution specific heat capacity (J/kgK); U (W/m^2K) and U_m (kg/m^2s) are heat transfer and mass transfer coefficients respectively, which are given by:

$$U = \left(\frac{1}{h_{air}} + \frac{\delta}{k_{mem}} + \frac{1}{h_{sol}}\right)^{-1} \quad (7)$$

$$U_m = \left(\frac{1}{h_{m,air}} + \frac{\delta}{k_{m,mem}}\right)^{-1} \quad (8)$$

Where h_{air} and h_{sol} are convective heat transfer coefficients in air and solution sides respectively (W/m^2K); $h_{m,air}$ is air side mass transfer coefficient (kg/m^2s); δ is membrane thickness (m); k_{mem} (W/mK) and $k_{m,mem}$(kg/ms) are membrane thermal conductivity and mass transfer conductivity respectively.

2.2. Normalization of governing equations

To simplify governing equations, several dimensionless numbers are defined:

Dimensionless length and height:

$$x^* = \frac{x}{L} \tag{9}$$

$$y^* = \frac{y}{H} \tag{10}$$

Dimensionless temperature:

$$T^* = \frac{T - T_{air,in}}{T_0} \tag{11}$$

Where T_0 is equal to $(T_{sol,in} - T_{air,in})$.

Dimensionless humidity ratio:

$$W^* = \frac{W - W_{air,in}}{W_0} \tag{12}$$

Where W_0 is equal to $(W_{sol,in} - W_{air,in})$.

m^* is mass flow rate ratio defined by:

$$m^* = \frac{\dot{m}_{sol}}{\dot{m}_{air}} \tag{13}$$

Cr^* is thermal capacity ratio and defined by:

$$Cr^* = \frac{(\dot{m}c_p)_{sol}}{(\dot{m}c_p)_{air}} \tag{14}$$

h^* is operating factor defined by:

$$h^* = \frac{W_0}{T_0}\frac{h_{fg}}{c_{p,air}} \tag{15}$$

NTU and NTU_m are numbers of heat and mass transfer respectively, which are defined by:

$$NTU = \frac{UA}{(\dot{m}c_p)_{air}} \tag{16}$$

$$NTU_m = \frac{U_m A}{\dot{m}_{air}} \tag{17}$$

Where A is total membrane area (m^2).

Then the governing equations (1)-(4) are normalized as:

$$\frac{\partial T^*_{sol}}{\partial y^*} + NTU_m h^* \frac{1}{Cr^*}\left(W^*_{sol,mem} - W^*_{air}\right) + NTU\frac{1}{Cr^*}(T^*_{sol} - T^*_{air}) = 0 \tag{18}$$

$$\frac{\partial X_{sol}}{\partial y^*} + NTU_m \frac{1}{m^*} W_0 (1 + X_{sol})(W^*_{sol,mem} - W^*_{air}) = 0 \tag{19}$$

$$\frac{\partial T^*_{air}}{\partial x^*} - NTU(T^*_{sol} - T^*_{air}) = 0 \tag{20}$$

$$\frac{\partial W^*_{air}}{\partial x^*} - NTU_m\left(W^*_{sol,mem} - W^*_{air}\right) = 0 \tag{21}$$

2.3. Boundary conditions

Boundary conditions for the solution side are:

$${T_{sol}}^* = 1,\ \text{at } y^*=0 \tag{22}$$

$$X_{sol} = X_{sol,in},\ \text{at } y^*=0 \tag{23}$$

While the air side boundary conditions are:

$$T_{air}{}^{*} = 0, \text{ at } x^{*}=0 \tag{24}$$

$$W_{\mathrm{air}}{}^{*} = 0, \text{ at } x^{*}=0 \tag{25}$$

2.3.1. Heat transfer boundary condition on membrane surface

Heat transfer boundary condition is based on thermal energy balance through the membrane:

$$h_{sol}\left(T_{sol} - T_{sol,mem}\right) = U\left(T_{sol,mem} - T_{air}\right) + h_{fg}U_m\left(W_{sol,mem} - W_{air}\right) \tag{26}$$

Eq. (26) can be normalized as:

$$NTU_{sol}\left(T^{*}_{sol} - T^{*}_{sol,mem}\right) = NTU\left(T^{*}_{sol,mem} - T^{*}_{air}\right) + NTU_m h^{*}\left(W^{*}_{sol,mem} - W^{*}_{air}\right) \tag{27}$$

Where NTU_{sol} is number of heat transfer unit in solution side and defined by:

$$NTU_{sol} = \frac{h_{sol}A}{(\dot{m}c_p)_{air}} \tag{28}$$

2.3.2. Mass transfer boundary condition on membrane surface

Similarly, mass transfer boundary condition is based on mass balance through the membrane:

$$U_m\left(W_{sol,mem} - W_{air}\right) = h_{m,sol}\left(C_{sol,mem} - C_{sol}\right) \tag{29}$$

Eq. (29) can be normalized as:

$$NTU_m W_0\left(W^{*}_{sol,mem} - W^{*}_{air}\right) = NTU_{m.sol}\left(C_{sol,mem} - C_{sol}\right) \tag{30}$$

Where $C_{sol,mem}$ is solution concentration in the interface between the solution and membrane; $NTU_{m.sol}$ is number of mass transfer unit in the solution side, which is defined by:

$$NTU_{m.sol} = \frac{h_{m,sol}A}{\dot{m}_{air}} \tag{31}$$

Where $h_{m,sol}$ is solution side mass transfer coefficient (kg/m^2s).

2.4. Air and desiccant solution properties

In the numerical modelling, the air specific humidity or humidity ratio ($kg/kg\ dry\ air$) is derived from its relative humidity by applying a correlation introduced in literature [32].

As for the solution, the relationship between the specific humidity and vapour pressure is given by [33]:

$$W_{sol} = 0.62198\frac{P_v}{P - P_v} \tag{32}$$

Where P is atmospheric pressure (Pa), P_v is equilibrium vapour pressure of desiccant solution (Pa), which is a function of T_{sol} and C_{sol} ($P_v = f(T_{sol}, C_{sol})$). This correlation is given by [34]:

$$Log\ P_v = KI\left[A - \frac{B}{T - E_s}\right] + \left[C - \frac{D}{T - E_s}\right] \tag{33}$$

Where P_v is solution equilibrium vapour pressure (kPa), K is an electrolyte parameter relating to solute; A, B, C, D and E_s are parameters regarding to solvent. A psychrometric chart of LiCl solution is shown in Fig. 2.

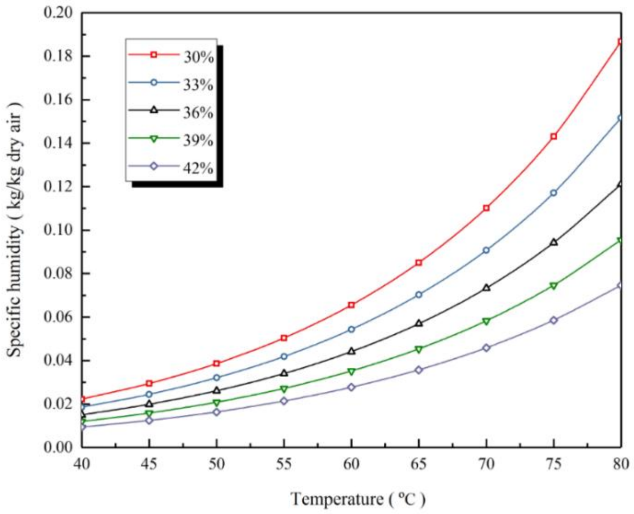

Fig. 2. Psychrometric chart of LiCl.

The desiccant solution and air transport properties used in the mathematical modelling are listed in Table 1.

Table 1

Air and desiccant solution transport properties.

Symbol	Unit	Value
k_{air}	W/mK	0.03
k_{sol}	W/mK	0.53
D_{air}	m^2/s	2.46×10^{-5}
D_{sol}	m^2/s	0.892×10^{-2}
$c_{p,air}$	J/kgK	1020
$c_{p,sol}$	J/kgK	3200
ρ_{air}	kg/m^3	1.29
ρ_{sol}	kg/m^3	1247

3. Performance evaluation

3.1. Solution side effectiveness for regenerator

Effectiveness is the most important parameter used to evaluate the performance of a heat and mass exchanger [35]. There are three types of effectiveness: sensible effectiveness (ε_{sen}), latent effectiveness (ε_{lat}) and total effectiveness (ε_{tot}). ε_{sen} is the ratio between the actual and maximum possible rates of sensible heat transfer in a heat exchanger, ε_{lat} is the ratio between the actual and maximum possible moisture transfer rates in a mass exchanger, and ε_{tot} is the ratio between the actual and maximum possible energy (enthalpy) transfer rates in a heat and mass exchanger. Air side effectiveness have been widely used for the dehumidification performance evaluation. In the regeneration process where the main focus is on desiccant solution, the air side effectiveness cannot reflect the regenerator performance correctly, thus the solution side effectiveness for regenerator are introduced referring to literature [31]:

$$\varepsilon_{sol,sen} = \frac{(\dot{m}c_p)_{sol}(T_{sol,in}-T_{sol,out})-\dot{m}_{desi}h_{fg}(X_{sol,in}-X_{sol,out})}{(\dot{m}c_p)_{min}(T_{sol,in}-T_{air,in})} \quad (34)$$

$$\varepsilon_{sol,lat} = \frac{\dot{m}_{desi} h_{fg}(X_{sol,in} - X_{sol,out})}{\dot{m}_{min} h_{fg}(W_{sol,in} - W_{air,in})} \quad (35)$$

$$\varepsilon_{sol,tol} = \frac{(\dot{m}c_p)_{sol}(T_{sol,in} - T_{sol,out})}{(\dot{m}c_p)_{min}(T_{sol,in} - T_{air,in}) + \dot{m}_{min} h_{fg}(W_{sol,in} - W_{air,in})} \quad (36)$$

Where the subscripts "in" and "out" represent inlet and outlet respectively. $\dot{m}_{desi}$ is desiccant flow rate (kg/s), which can be obtained by:

$$\dot{m}_{desi} = \frac{\dot{m}_{sol}}{1 + X_{sol}} \quad (37)$$

3.2. Solution side moisture flux rate (MFR)

Moisture removal rate (MRR) has been used to evaluate the amount of moisture being removed by the air from diluted liquid desiccant solution, or the amount of moisture being absorbed by concentrated solution from humid air [29, 36-38]. In this study with the main focus on desiccant solution, a similar index so called solution side moisture removal rate is introduced and expressed as:

$$MRR = \dot{m}_{desi}(X_{sol,in} - X_{sol,out}) \quad (38)$$

Then, another important index so called solution side moisture flux rate is defined:

$$MFR = \frac{MRR}{U_m A} = \frac{\dot{m}_{desi}(X_{sol,in} - X_{sol,out})}{U_m A} \quad (39)$$

As can been seen from the above equation, MFR is the ratio between moisture removal rate MRR and membrane overall mass transfer conductance. MFR is generally used for performance evaluation rather than MRR, because it is independent of the size of the regenerator. It only depends on the inlet condition, which would make results more general [30].

3.3. Solution temperature decrease rate (TDR)

Apart from re-concentration of the liquid desiccant solution, the lower solution temperature is preferred. Lower solution temperature would make dehumidification more effective. Thus, the index so called solution temperature decrease rate (TDR) is applied to evaluate the sensible performance of regeneration, which is defined as:

$$TDR = \frac{T_{sol,in} - T_{sol,out}}{T_{sol,in}} \quad (40)$$

4. Simulation procedure

4.1. Discretization of governing equations

Finite difference method is used to solve governing equations which are discretized by a forward difference scheme:

$$T^*_{sol\,(m+1,n)} - T^*_{sol\,(m,n)} + dy^* NTU_m h^* Cr\left[W^*_{sol,mem\,(m+1,n)} - W^*_{air\,(m+1,n)}\right] + dy^* NTU Cr\left[T^*_{sol\,(m+1,n)} - T^*_{air\,(m+1,n)}\right] = 0 \quad (41)$$

$$X_{sol\,(m+1,n)} - X_{sol\,(m,n)} + dy^{*}m^{*}W_0 NTU_m\left[1 + X_{sol\,(m+1,n)}\right]\left[W^{*}_{sol,mem\,(m+1,n)} - W^{*}_{air\,(m+1,n)}\right] = 0 \tag{42}$$

$$T^{*}_{air\,(m,n+1)} - T^{*}_{air\,(m,n)} - dx^{*}NTU\left[T^{*}_{sol\,(m,n+1)} - T^{*}_{air\,(m,n+1)}\right] = 0 \tag{43}$$

$$W^{*}_{air\,(m,n+1)} - W^{*}_{air\,(m,n)} - dx^{*}NTU_m\left[W^{*}_{sol,mem\,(m,n+1)} - W^{*}_{air(m,n+1)}\right] = 0 \tag{44}$$

Where m is number of girds in x direction, and n is number of girds in y direction. Governing equations are solved in Matlab iteratively until converged. Numerical tests have been conducted to determine the grid size for guaranteeing the accuracy of numerical results. It has been found that 30×60 grids are adequate in this study, the result difference is less than 1.0% compared with 50×100 grids. The numerical uncertainty is 1.0%.

4.2. Numerical solving scheme

The solution procedure used to solve interacted governing equations is illustrated in Fig. 3.

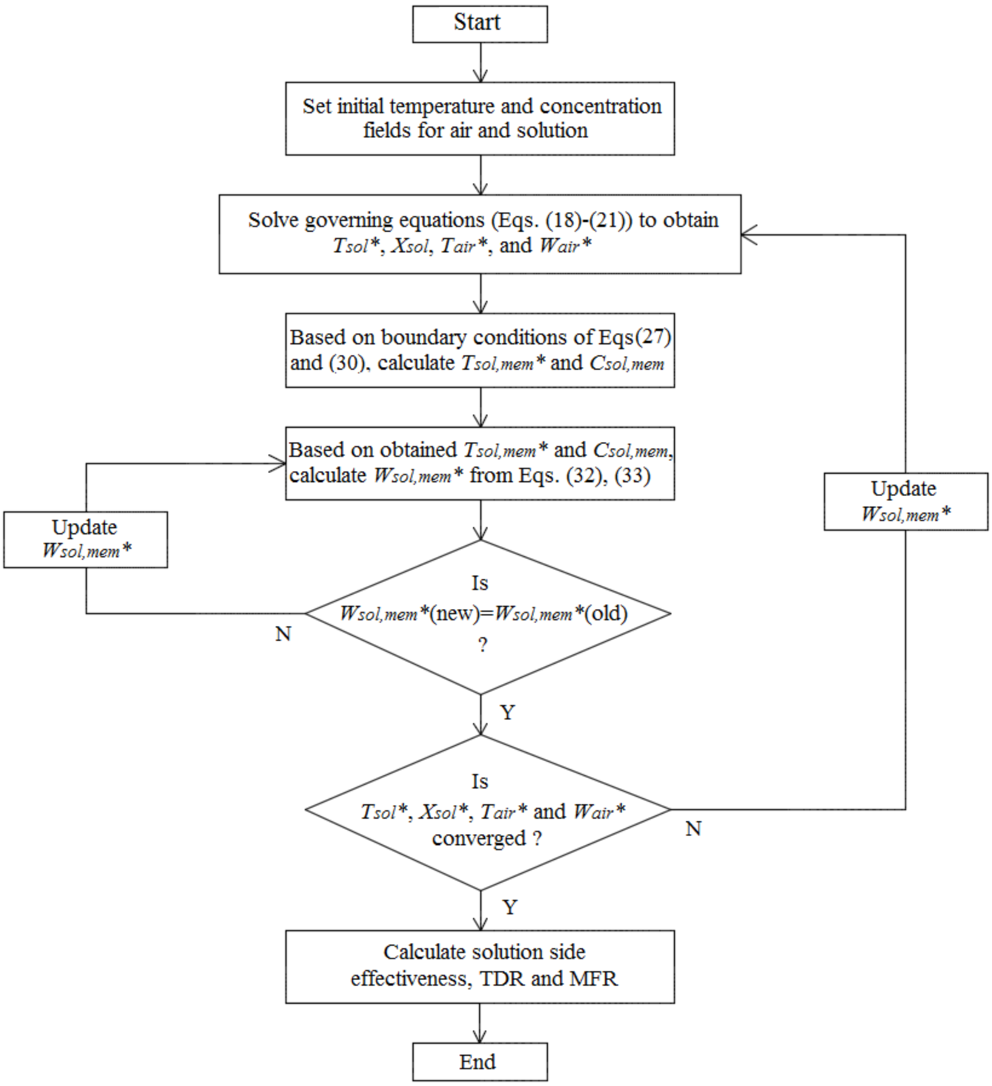

Fig. 3. Flow chart for the solution procedure

5. Experimental test

A membrane-based heat and mass exchanger test facility is built in the laboratory. Extensive experiments have been carried out to investigate the regeneration performance under different operating conditions. The schematic of the test rig is shown in Fig. 4.

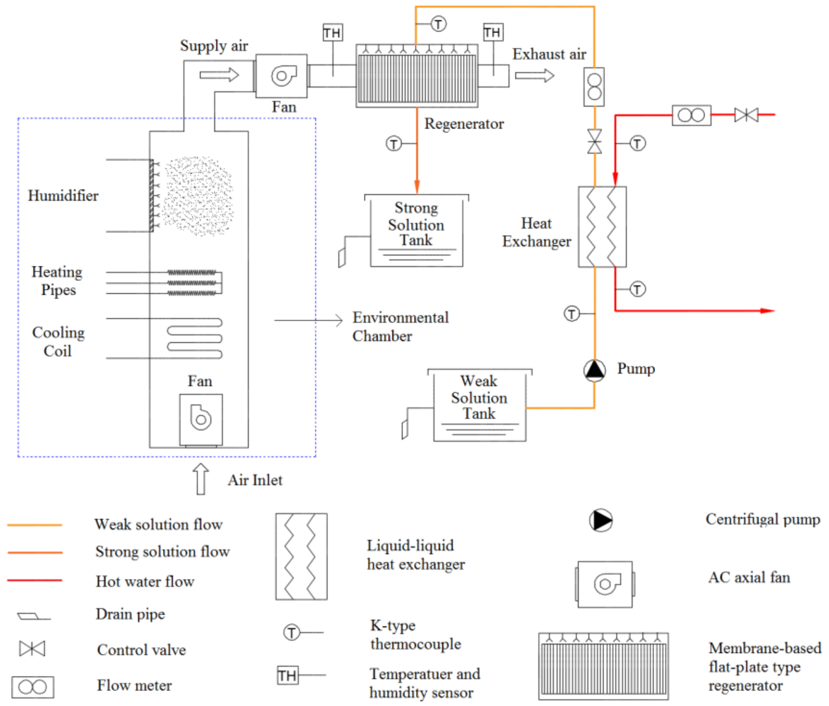

Fig. 4. Schematic diagram of the laboratory test rig

The test rig mainly consists of one flat-plate membrane-based regenerator, one weak solution tank, one strong solution tank, one AC axial fan and one liquid-liquid heat exchanger. The regenerator is the most important unit in the system, which has a dimension of 410mm (L) x 230mm (W) x 210mm (H) with 11 air channels and 11 solution channels. Three gauze layers are paved on the top surface of the regenerator to ensure even solution distribution. The regenerator specifications and membrane physical properties are given in Table 2.

Table 2

Regenerator specifications and membrane physical properties.

Symbol	Unit	Value
L	m	0.41
W	m	0.23
H	m	0.21
d_{air}	m	0.0077
d_{sol}	m	0.0043
δ_{mem}	m	0.5×10^{-3}
k_{mem}	W/mK	0.3
$k_{m,mem}$	kg/ms	3.87×10^{-6}

The regenerator supply air is provided by an environmental chamber, which is equipped with a cooling coil, three heating pipes and one humidifier. The supply air with desired condition flows into the regenerator, where both its temperature and moisture content are increased by hot and diluted desiccant solution. The air flow rate is controlled by adjusting an AC axial fan rotation speed (ebm-papst Mulfingen GmbH & Co. KG). The air velocity is measured at the air duct outlet by a thermo-anemometer (Testo 405) with the measuring range up to 10 m/s. In the open liquid loop, lithium chloride (LiCl) is used as the desiccant in the system. The diluted desiccant solution is supplied by one centrifugal magnetic pump (15W centrifugal magnetically driven type with flow rate range of 0-10L/min) from the weak solution tank, and its flow rate is controlled and measured by one liquid flow indicator (Parker UCC PET 1-15 L/min). The re-concentrated desiccant solution is then collected by the strong solution tank. The weak desiccant solution temperature is controlled by a hot water supply system with the supply water temperature range of 20℃ to 80℃. The hot water flow rate is controlled and measured by another liquid flow indicator (Parker FM 26 122 212 0.5-4.5 L/min). For the air temperature and humidity measurements, the air inlet and outlet are instrumented with humidity and temperature sensors (Sensirion Evaluation KIT EK-H4). The desiccant solution and hot water temperatures are measured by K-type thermocouples, which are connected to a DT500 data logger for data acquisition. The regenerator, heat exchanger, solution tanks, pipes and air ducts are well insulated to minimize the environment influence. All measurement devices and their accuracies are listed in Table 3. Uncertainty analysis has been conducted for all experimental data by applying a method of propagation [39] to estimate uncertainties for experimental data.

Table 3

Measurement devices and uncertainties.

Device	Measurement	Range	Uncertainty
Testo thermos-anemometer	Air velocity	0-10 m/s	$\pm 5\%$
Sensiron Evaluation KIT EK-H4	Temperature	-40-125 ℃	$\pm 0.4\%$
	Relative humidity	0-100 %	$\pm 3\%$
K-type thermocouple probe	Temperature	0-1100 ℃	$\pm 0.75\%$
DT500 Datalogger	Data acquisition	-	$\pm 0.15\%$
Parker UCC PET liquid flow indicator	Solution flow rate	1-15 L/min	$\pm 5\%$
Parker FM 26 122 212 liquid flow indicator	Water flow rate	2-22 L/min	$\pm 5\%$

6. Model validation

The experimental data are used to validate the numerical simulation results. 44 groups of experimental data under different operating conditions are adopted in this study. The experiment consists of two stages. In the first stage, 22 groups of tests are conducted to validate the solution side effectiveness (solution side sensible effectiveness $\varepsilon_{sol,sen}$, latent effectiveness $\varepsilon_{sol,lat}$, and total effectiveness $\varepsilon_{sol,tot}$). The operating conditions (i.e. NTU, m^* et al.), as well as numerically calculated and measured results of effectiveness are listed in Table 4. In the second stage, another 22 groups of tests are carried out to validate the solution side temperature decrease rate (TDR) and moisture flux rate (MFR). The comparisons between numerical and experimental results are given in Table 5.

Table 4

Comparisons between numerical and experimental results for solution side effectiveness

Operating conditions								Comparisons								
NTU	m*	m_{air} (kg/s)	m_{sol} (kg/s)	$T_{sol,in}$ (℃)	$C_{sol,in}$ (%)	$T_{air,in}$ (℃)	$W_{air,in}$ (kg/kg)	$\varepsilon_{sol,sen,num}$	$\varepsilon_{sol,sen,exp}$	Error (%)	$\varepsilon_{sol,lat,num}$	$\varepsilon_{sol,lat,exp}$	Error (%)	$\varepsilon_{sol,tot,num}$	$\varepsilon_{sol,tot,exp}$	Error (%)
2	1	0.1234	0.1234	60	35	30	12.6	0.6628	0.622	6.156	0.2893	0.246	14.967	0.3881	0.342	11.878
6	1	0.0411	0.0411	60	35	30	12.6	0.7594	0.710	6.505	0.4311	0.388	9.998	0.5179	0.470	9.249
10	1	0.0247	0.0247	60	35	30	12.6	0.7752	0.719	7.250	0.4835	0.429	11.272	0.5606	0.508	9.383
2	2	0.1234	0.2469	60	35	30	12.6	0.7553	0.729	3.482	0.3767	0.334	11.335	0.4769	0.435	8.786
6	2	0.0411	0.0822	60	35	30	12.6	0.8968	0.860	4.103	0.6079	0.566	6.893	0.6843	0.636	7.058
10	2	0.0247	0.0494	60	35	30	12.6	0.9293	0.898	3.368	0.6963	0.658	5.501	0.7580	0.729	3.826
2	3	0.1234	0.3703	60	35	30	12.6	0.7914	0.785	0.809	0.4166	0.392	5.905	0.5157	0.472	8.474
6	3	0.0411	0.1234	60	35	30	12.6	0.9482	0.927	2.236	0.6905	0.671	2.824	0.7587	0.741	2.333
10	3	0.0247	0.0741	60	35	30	12.6	0.9852	0.955	3.065	0.7918	0.757	4.395	0.8430	0.825	2.135
8	2	0.0309	0.0617	50	35	30	12.6	0.9502	0.926	2.547	0.7386	0.706	4.414	0.8130	0.778	4.305
8	2	0.0309	0.0617	55	35	30	12.6	0.9329	0.909	2.562	0.7024	0.669	4.755	0.7724	0.741	4.065
8	2	0.0309	0.0617	60	35	30	12.6	0.9156	0.887	3.124	0.6602	0.623	5.635	0.7278	0.695	4.507
8	2	0.0309	0.0617	65	35	30	12.6	0.8981	0.861	4.131	0.6136	0.573	6.617	0.6792	0.639	5.919
8	2	0.0309	0.0617	70	35	30	12.6	0.8803	0.849	3.556	0.5636	0.512	9.155	0.6272	0.583	7.047
8	2	0.0309	0.0617	60	35	26	12	0.8335	0.813	2.460	0.4617	0.421	8.815	0.5679	0.529	6.850
8	2	0.0309	0.0617	60	35	28	12	0.8319	0.808	2.873	0.4635	0.417	10.032	0.5643	0.522	7.496
8	2	0.0309	0.0617	60	35	30	12	0.8302	0.756	8.938	0.4654	0.425	8.681	0.5606	0.520	7.242
8	2	0.0309	0.0617	60	35	32	12	0.8282	0.762	7.993	0.4672	0.398	14.812	0.5567	0.510	8.389
8	2	0.0309	0.0617	60	35	34	12	0.8258	0.779	5.667	0.4691	0.414	11.746	0.5527	0.508	8.088
8	2	0.0309	0.0617	60	35	30	9	0.8280	0.753	9.058	0.4680	0.419	10.470	0.5564	0.495	11.035
8	2	0.0309	0.0617	60	35	30	12	0.8302	0.756	8.938	0.4654	0.425	8.681	0.5606	0.510	9.026
8	2	0.0309	0.0617	60	35	30	15	0.8324	0.761	8.578	0.4623	0.397	14.125	0.5653	0.509	9.959

Table 5

Comparisons between numerical and experimental results for TDR and MFR

Operating conditions								Comparisons					
NTU	m*	m_{air} (kg/s)	m_{sol} (kg/s)	$T_{sol,in}$ (℃)	$C_{sol,in}$ (%)	$T_{air,in}$ (℃)	$W_{air,in}$ (kg/kg)	TDR_{num}	TDR_{exp}	Error (%)	MFR_{num}	MFR_{exp}	Error (%)
2	2	0.1234	0.2469	60	35	30	12.6	0.1437	0.131	8.838	0.0162	0.015	7.407
6	2	0.0411	0.0822	60	35	30	12.6	0.2062	0.196	4.947	0.0087	0.008	8.046
10	2	0.0247	0.0494	60	35	30	12.6	0.2283	0.220	3.636	0.0056	0.005	10.254
2	1	0.1234	0.1234	60	35	30	12.6	0.2338	0.221	5.475	0.0124	0.011	11.290
2	2	0.1234	0.2469	60	35	30	12.6	0.1437	0.127	11.797	0.0162	0.015	7.407
2	3	0.1234	0.3703	60	35	30	12.6	0.1036	0.092	11.197	0.0179	0.017	5.028
8	2	0.0309	0.0617	50	35	30	12.6	0.1474	0.132	10.448	0.0035	0.003	14.286
8	2	0.0309	0.0617	55	35	30	12.6	0.1843	0.176	4.504	0.0057	0.005	12.281
8	2	0.0309	0.0617	60	35	30	12.6	0.2192	0.198	9.672	0.0068	0.006	11.493
8	2	0.0309	0.0617	65	35	30	12.6	0.2525	0.242	4.158	0.0092	0.009	2.174
8	2	0.0309	0.0617	70	35	30	12.6	0.2843	0.266	6.437	0.0115	0.010	13.043
8	2	0.0309	0.0617	60	33	26	12	0.2411	0.232	3.774	0.0082	0.008	2.439
8	2	0.0309	0.0617	60	35	28	12	0.2192	0.196	10.584	0.0069	0.006	13.493
8	2	0.0309	0.0617	60	37	30	12	0.1957	0.178	9.044	0.0057	0.005	12.667
8	2	0.0309	0.0617	60	35	26	12	0.0598	0.056	6.355	0.0202	0.019	5.941
8	2	0.0309	0.0617	60	35	28	12	0.0584	0.055	5.822	0.0203	0.019	6.404
8	2	0.0309	0.0617	60	35	30	12	0.0571	0.054	5.429	0.0203	0.019	6.404
8	2	0.0309	0.0617	60	35	32	12	0.0557	0.053	4.847	0.0204	0.020	1.961
8	2	0.0309	0.0617	60	35	34	12	0.0543	0.051	6.077	0.0205	0.019	7.317
8	2	0.0309	0.0617	60	35	30	9	0.0602	0.057	5.316	0.0222	0.021	5.405
8	2	0.0309	0.0617	60	35	30	12	0.0571	0.054	5.429	0.0203	0.019	6.404
8	2	0.0309	0.0617	60	35	30	15	0.0539	0.048	10.946	0.0185	0.018	2.703

It can be seen in Table 4 that the numerical modelling results of ε_{sen}, ε_{lat} and ε_{tot} generally agree well with the experimental data. The maximum discrepancies between numerical results and experimental data for $\varepsilon_{sol,sen}$, $\varepsilon_{sol,lat}$ and $\varepsilon_{sol,tot}$ are 9.058%, 14.967% and 11.878%

respectively. The maximum differences for TDR and MFR are 11.797% and 14.286% respectively, as indicated in Table 5. It should be emphasized that under the same NTU, the discrepancy reduces with the solution mass flow rate. For instance, under $NTU = 6$, the differences between numerical and experimental results decrease from 6.505% to 2.236% for $\varepsilon_{sol,sen}$, 9.998% to 2.824% for $\varepsilon_{sol,lat}$, and 9.249% to 2.333% for $\varepsilon_{sol,tot}$ respectively when the solution mass flow rate increases from 0.0411 kg/s to 0.1234 kg/s. This is because the lower of solution mass flow rate, the greater influence of solution mal-distribution on the effectiveness. The numerical modelling results and experimental data have similar variation trends, an acceptable agreement between them is achieved, meaning the developed model predicts the performance rather accurately and is successful to simulate the operating characteristics of the cross-flow flat-plate membrane-based regenerator.

7. Results and discussion

7.1. Temperature and humidity fields

Under each operating condition, temperature and humidity fields of the air and solution channels and the membrane surface are obtained after all governing equations are converged. The distributions of temperature and concentration in the solution channel, and the temperature and humidity ratio fields in the air channel and membrane surface under $NTU = 8$ and $m^* = 2$ are plotted in Fig. 5. The inlet temperatures of the diluted solution and air are 60 ℃ and 30 ℃ respectively, while the inlet solution concentration and air relative humidity are set as 35% and 50% ($W_{air,in} = 12.6\, g/kg\ dry\ air$) respectively. It can be observed in Fig. 5(a) and (b) that the solution has the lowest temperature (35.4 ℃) and highest concentration (35.51%) at the left bottom corner of the regenerator. This is due to the fact that the hot and diluted solution at the left bottom side interacts with the cooler and dryer supply air. Similar case can be found in the air channel, the air reaches its highest temperature (60 ℃) and humidity ratio (45.7 $g/kg\ dry\ air$) at the right top corner since the air is heated and humidified along the length of the regenerator. Moreover, Fig. 5 (e) and (f) illustrate the temperature and humidity boundary conditions on the membrane surface, it is clear that the boundary condition is neither uniform temperature nor uniform humidity ratio. The temperature and humidity ratio are non-uniform and two-dimensional profiles, both of them increase along the diagonal line of the membrane surface.

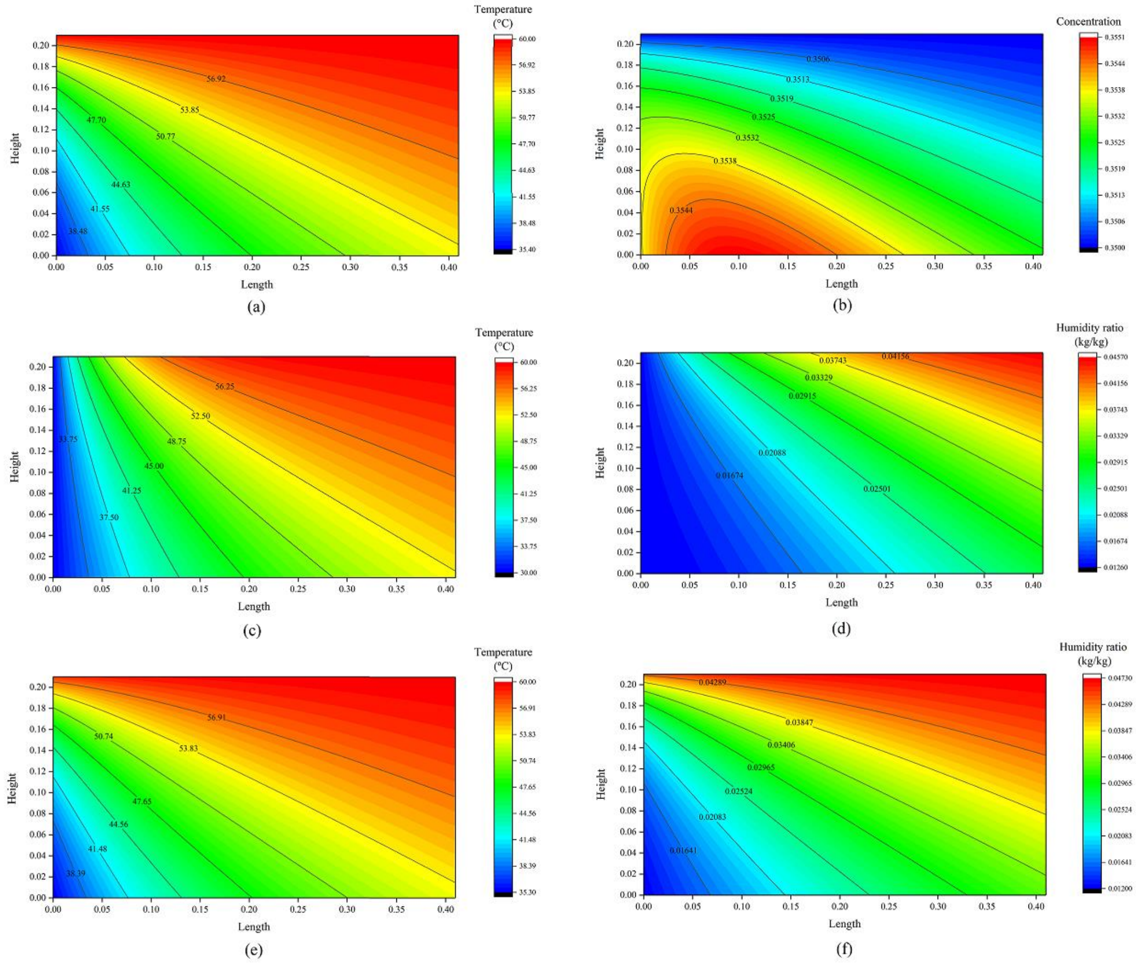

Fig. 5. (a) Solution temperature field; (b) Solution concentration field; (c) Air temperature field; (d) Air humidity ratio field; (e) Temperature field on membrane surface; (f) Humidity ratio field on membrane surface

7.2. Effects of dimensionless parameters

In this section, influences of two dimensionless parameters: NTU and m^* on the regeneration performance are addressed. NTU has been considered as a critical parameter with the most significant impact on the dehumidification system [14, 40]. Compared to the flow rate, the non-dimensional group NTU is a comprehensive indicating parameter because it is independent of the channel geometric properties. In numerical simulation, NTU is changed by adjusting air mass flow rate, while the solution mass flow rate is changed proportionally to maintain a constant m^* accordingly.

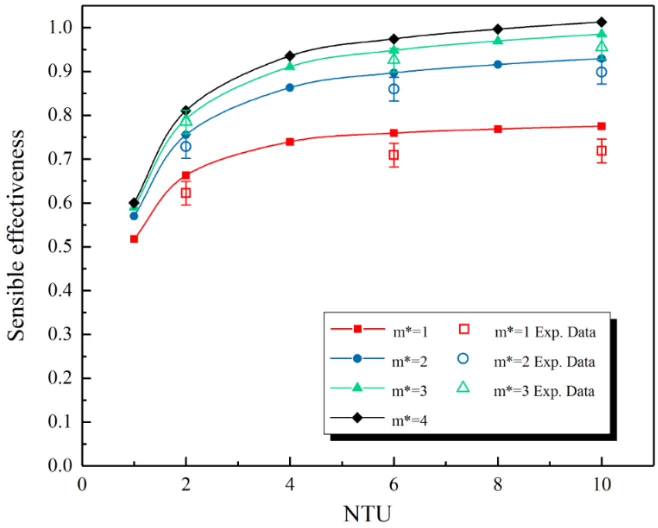

Fig. 6. Sensible effectiveness variations with NTU under different m^*

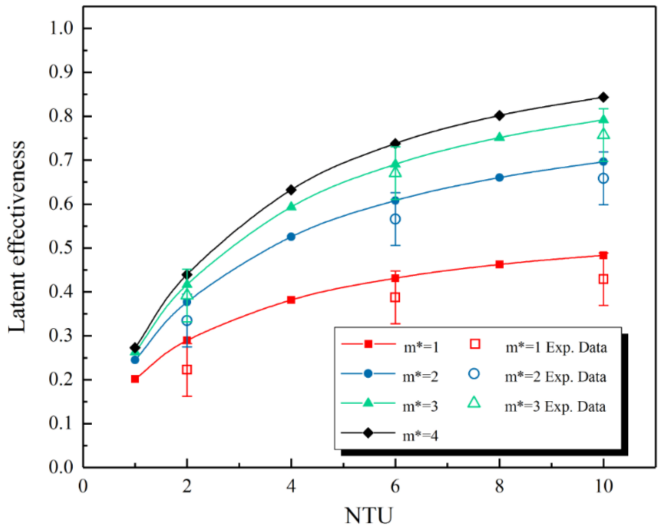

Fig. 7. Latent effectiveness variations with NTU under different m^*

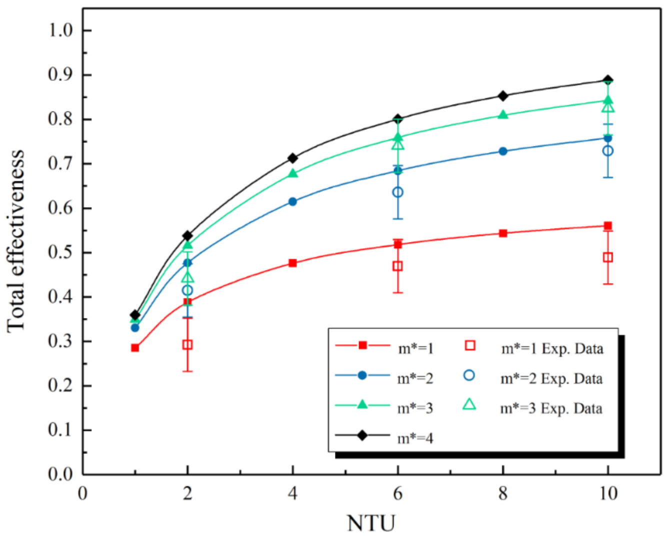

Fig. 8. Total effectiveness variations with NTU under different m^*

Influences of NTU on the regenerator effectiveness are analysed at first. Variations of the effectiveness with NTU under $m^* = 1,2,3,4$ are plotted in Figs. 6-8. It can be seen in these figures that under the same m^*, the sensible effectiveness always has the highest value among three effectiveness, while the latent effectiveness is the lowest one and the total effectiveness is the middle one. For example, under $m^* = 1$, the sensible effectiveness varies from 0.5179 to 0.7752 when NTU rises from 1 to 10. In the meanwhile, the latent effectiveness changes from 0.2017 to 0.4835 and the total effectiveness increases from 0.2854 to 0.5606. It is obvious that all effectiveness are significantly affected by NTU, and can be improved by increasing NTU. A critical value of NTU exists and is defined as NTU_{crit}, which is equal to 4 in this case. Increasing NTU beyond NTU_{crit} would not enhance the regeneration performance efficiently. For instance, under $m^* = 1$, the sensible effectiveness is increased by 42.79% (from 0.5179 to 0.7395) when NTU changes from 1 to 4. After NTU exceeding 4 the variation of the sensible effectiveness trends to level off, and it is only increased by 4.83% (from 0.7395 to 0.7752) when NTU rises from 4 to 10. Therefore increasing NTU beyond NTU_{crit} would not enhance the effectiveness effectively. This effect is relatively inconspicuous for the latent and total effectiveness. Take the latent effectiveness as an example, under $m^* = 1$, it is increased by 89.09% and 26.77% when NTU rises from 1 to 4 and from 4 to 10 respectively. Furthermore, when m^* is relatively low, the growth extent of the effectiveness with NTU is not as obvious as that when m^* is high. Take the latent effectiveness as an example, under $m^* = 1$, the latent effectiveness is increased by 0.2818 (from 0.2017 to 0.4835) when NTU changes from 1 to 10, while it is increased by 0.5707 (from 0.2728 to 0.8435) under $m^* = 4$, almost twice as that under $m^* = 1$. Similar cases can also be found for the sensible and total effectiveness.

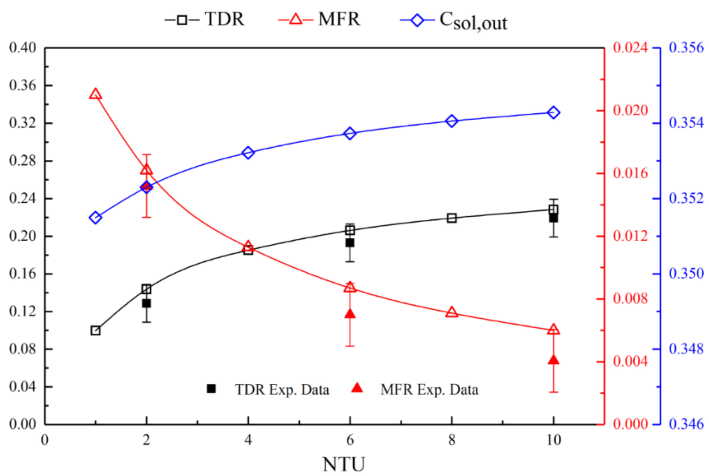

Fig. 9. Influences of NTU on TDR, MFR and $C_{sol,out}$

Apart from the solution side effectiveness, the solution side TDR and MFR have also been applied for regeneration performance evaluation. The variations of TDR, MFR and solution outlet concentration $C_{sol,out}$ with NTU under $m^* = 2$ are shown in Fig. 9. According to this figure, TDR increases from 0.0997 to 0.2283 when NTU changes from 1 to 10, meaning the solution cooling effect is enhanced. Meanwhile, MFR is dramatically decreased from 0.021 to 0.006. This is because the air mass rate decreases (from 0.2469 kg/s to 0.0247 kg/s) with NTU. When m^* remains unchanged, the corresponding solution flow rate should decrease as well. Based on Eq. (37), the desiccant mass flow rate is then decreased significantly (from 0.1728 kg/s to 0.0173 kg/s), and as a result MFR is deteriorated. However, $C_{sol,out}$ is increased from 0.351 to 0.355. The low vapour pressure in the air channel would be nearly constant as the air and solution flow rates decrease. Consequently, the mass transfer between the air and solution is enhanced, which leads to the increase of the solution outlet concentration.

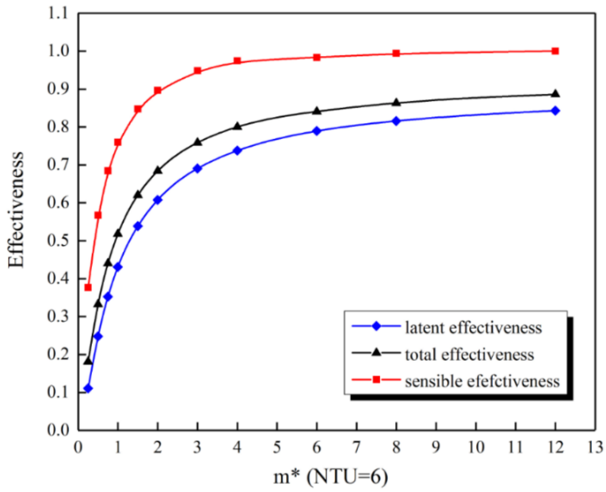

Fig. 10. Variations of effectiveness with m^* under $NTU = 6$

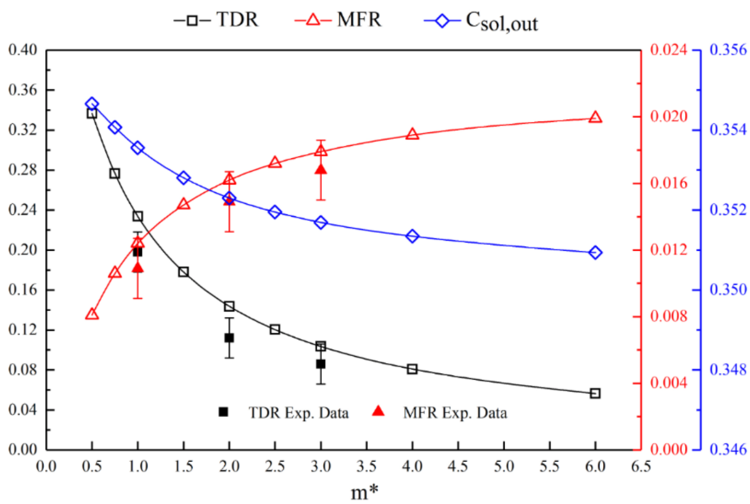

Fig. 11. Influences of m^* on TDR, MFR and $C_{sol,out}$

m^* is another important dimensionless parameter affecting regeneration performance, which is the relative mass flow rate of two fluids in the regenerator. m^* can be controlled by adjusting the solution mass flow rate while keeping the air mass flow rate constant under each NTU. Variations of the effectiveness, TDR, MFR and $C_{sol,out}$ with m^* under $NTU = 6$ are shown in

Figs. 10 and 11. Clearly, under the same NTU, the sensible effectiveness is continuously the highest one, while the latent effectiveness is the lowest one and the total effectiveness is the middle one. A critical indicator Cr^*_{crit} has been introduced [40, 41], all effectiveness increase with Cr^* and are more sensitive before Cr^* reaching Cr^*_{crit}. Similarly a critical value of m^* is defined as m^*_{crit}. m^* is proportional to Cr^*, but it is a more straightforward parameter for the system. The effectiveness are more sensitive to m^* when m^* is lower than m^*_{crit}. As shown in Fig. 10, m^*_{crit} is 2 in this study, and once m^* exceeds m^*_{crit}, the gradients of all effectiveness changes become moderate gradually and only a slight variation can be observed. For example, the sensible effectiveness is improved by 0.5198 (from 0.377 to 0.8968) when m^* changes from 0.25 to 2. However, it is only increased by 0.0997 (from 0.8968 to 0.9965) when m^* keeps increasing to 12. Besides, as mentioned previously, the effects of NTU and m^* are interacted with each other. It can also be observed from Figs.6-8 that the effectiveness variations with m^* are more significant under high NTU, meaning the effectiveness cannot be improved effectively by increasing m^* when NTU is too low. For instance, the sensible, latent and total effectiveness are raised by 0.0825, 0.0711 and 0.0741 individually as m^* increases from 1 to 4 under $NTU = 1$. By contrast, these effectiveness are increased by 0.2376, 0.36 and 0.3277 respectively under $NTU = 10$.

Effects of m^* on TDR, MFR and $C_{sol,out}$ are demonstrated in Fig. 11. Compared with the effects of NTU as shown in Fig. 9, m^* has opposite influences on TDR, MFR and $C_{sol,out}$. Heat capacity rate of the solution become higher with the solution flow rate, which would cause less temperature reduction of the desiccant solution during the phase change process [36], meaning the solution outlet temperature is increased and TDR is reduced. For example, under $NTU = 6$, $T_{sol,out}$ rises from 41.28 ℃ to 50.86 ℃ as m^* increases from 1 to 3, resulting in the TDR decreases from 0.3120 to 0.1524. So the solution cooling effect is deteriorated. In the meanwhile, the solution outlet concentration is decreased as well. It can be noticed in Fig. 11 that $C_{sol,out}$ reduces slightly from 0.356 to 0.352. However, according to Eq. (37), increasing the solution mass flow rate would raise desiccant mass flow rate as well, which eventually improves MFR from 0.0035 to 0.0113. It is also noteworthy that similar to the effects of m^*_{crit} on the effectiveness, the variations of TDR, MFR and $C_{sol,out}$ also become steady after m^* reaching m^*_{crit}.

7.3. Effects of desiccant solution properties

Two solution properties: solution inlet temperature $T_{sol,in}$ and concentration $C_{sol,in}$ are investigated to clarify their influences on the regenerator effectiveness, TDR, MFR and $C_{sol,out}$. Variations of the regenerator effectiveness, TDR, MFR and $C_{sol,out}$ with $T_{sol,in}$ under different $C_{sol,in}$ are displayed in Figs. 12-15.

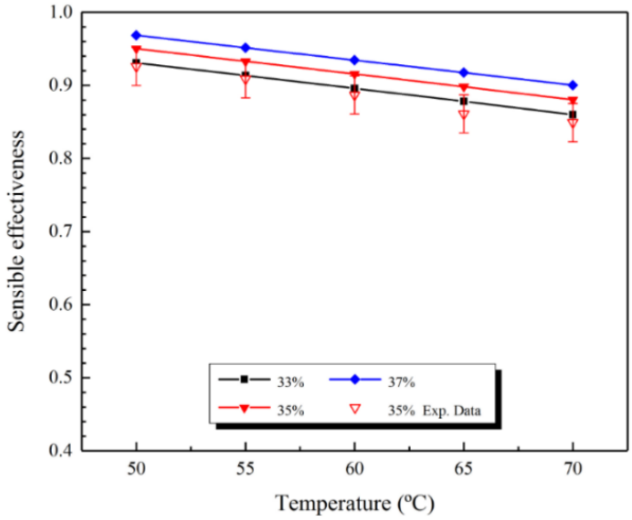

Fig. 12. Sensible effectiveness variations with $T_{sol,in}$ under different $C_{sol,in}$

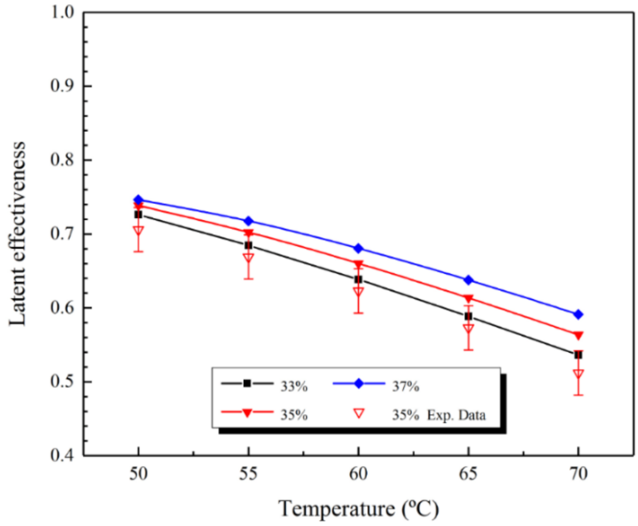

Fig. 13. Latent effectiveness variations with $T_{sol,in}$ under different $C_{sol,in}$

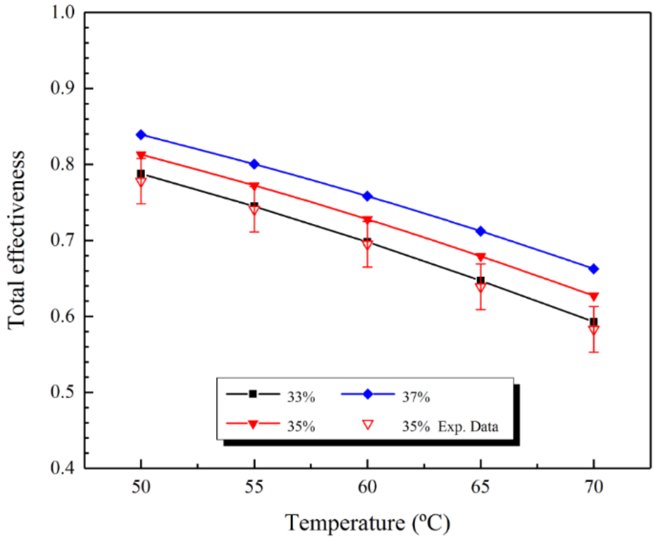

Fig. 14. Total effectiveness variations with $T_{sol,in}$ under different $C_{sol,in}$

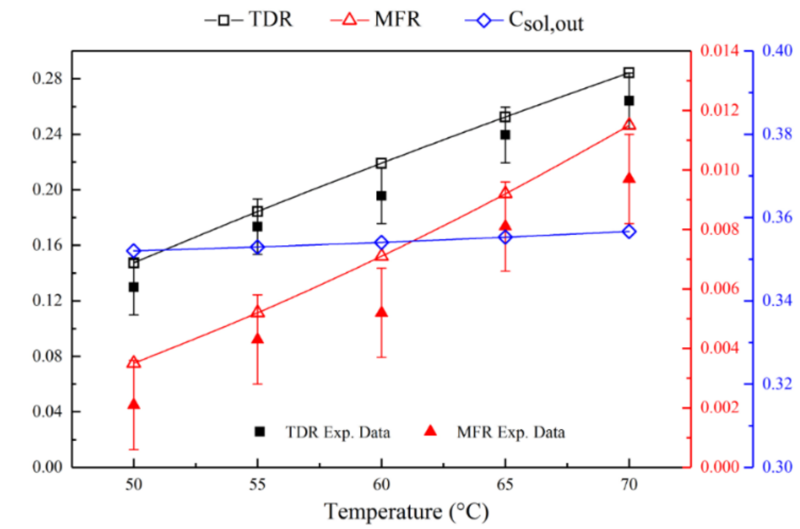

Fig. 15. Influences of $T_{sol,in}$ on TDR, MFR and $C_{sol,out}$

Solution temperature has great influence on the system performance as it is closely related to the solution surface vapour pressure. For the purpose of variable separation, NTU and m^* are set as 8 and 2 respectively. As shown in Figs. 12-14, under the same solution concentration, the sensible effectiveness is the highest among three effectiveness, while the latent effectiveness is the lowest and the total effectiveness is the middle. For example, under $C_{sol,in} = 33\%$, the sensible effectiveness varies from 0.9308 to 0.86 when $T_{sol,in}$ rises from 50 ℃ to 70 ℃. In the meanwhile, the latent effectiveness decreases from 0.7263 to 0.5362 and the total effectiveness changes from 0.7877 to 0.5931 respectively. All effectiveness decrease with $T_{sol,in}$. According to the definition of the solution side sensible effectiveness (as given in Eq. (34)), the absolute value of denominator in Eq. (34) increases with $T_{sol,in}$, so the sensible effectiveness is reduced moderately. Besides, as indicated in Fig. 2, the increase of $T_{sol,in}$ under the same $C_{sol,in}$ would result in high solution equilibrium humidity ratio. Based on the definition of the solution side latent effectiveness (as given in Eq. (35)), the absolute value of denominator in Eq. (35) increases with $T_{sol,in}$, this leads to the decrease of the latent effectiveness. Compared to the latent and total effectiveness, the sensible effectiveness is relatively less sensitive to $T_{sol,in}$. For instance, under $C_{sol,in} = 37\%$, increasing $T_{sol,in}$ from 50 ℃ to 70 ℃ would reduce the sensible effectiveness by 7.05% (from 0.9686 to 0.9003). By contrast, the latent and total effectiveness are reduced by 20.80% (from 0.7463 to 0.5911) and 21.05% (from 0.8393 to 0.6626) respectively. Despite the deterioration of all effectiveness with increasing $T_{sol,in}$, the higher $T_{sol,in}$, the higher solution equilibrium humidity ratio and vapour pressure. Consequently both heat and mass transfer potentials are strengthened, and these have been reflected clearly in Fig. 15, where TDR, MFR and $C_{sol,out}$ are all improved with $T_{sol,in}$.

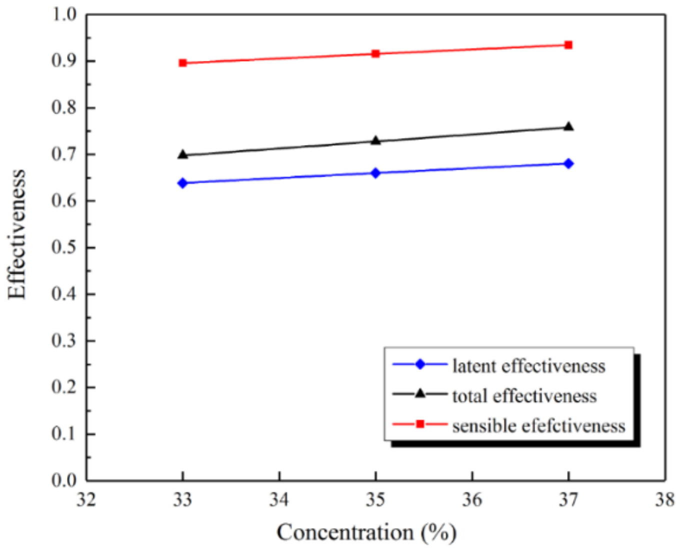

Fig. 16. Variations of effectiveness with $C_{sol,in}$ under $T_{sol,in} = 60°C$

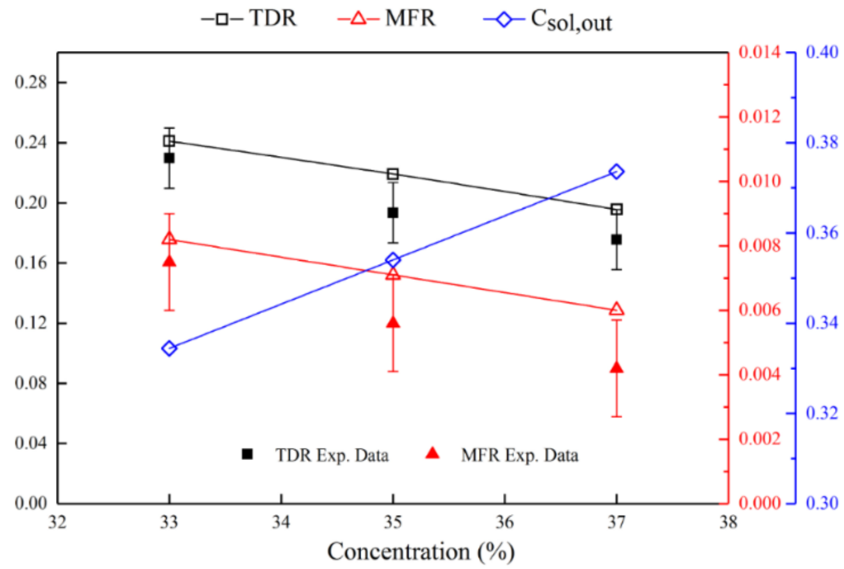

Fig. 17. Influences of $C_{sol,in}$ on TDR, MFR and $C_{sol,out}$

Apart from the solution inlet temperature, the solution inlet concentration also affects the regeneration performance since it is directly related to surface vapour pressure as well. Variations of the effectiveness, TDR, MFR and $C_{sol,out}$ with $C_{sol,in}$ under $T_{sol,in} = 60°C$ are shown in Figs. 16 and 17. As indicated in Fig. 16, the sensible effectiveness is again the highest among three, while the latent effectiveness is the lowest and the total effectiveness is the middle under the same $T_{sol,in}$. All effectiveness increase with $C_{sol,in}$ slightly. However the increase rates are insignificant compared with the effects of decreasing $T_{sol,in}$, meaning the regenerator is less sensitive to $C_{sol,in}$. For example, the sensible, latent and total effectiveness are only changed by 4.3%, 6.58% and 8.64% respectively when $C_{sol,in}$ rises from 33% to 37%. Based on Fig. 2, increasing the solution inlet concentration would decrease the solution equilibrium humidity ratio. Thus both the solution inlet mass fraction $X_{sol,in}$ and equilibrium humidity ratio

$W_{sol,in}$ in Eq. (35) are decreased. These effects offset with each other and eventually the latent effectiveness increases slightly. However, the decrease of the solution vapour pressure would reduce mass transfer potential. As a result, MFR is decreased as illustrated in Fig. 17. On the other hand, the reduction of mass transfer (latent heat transfer) would decrease heat absorption during the evaporation process in the solution channel. Thus $T_{sol,out}$ is increased and TDR is decreased as reflected in Fig. 17. As for the slight increase of the sensible effectiveness, this can be explained by the definition in Eq. (34), increasing $T_{sol,out}$ would decrease the absolute value of the total heat transfer, which is the first term in the numerator. In the meanwhile, the second term in the numerator is deteriorated as well, which represents the latent heat transfer. Consequently, the sensible effectiveness increases slightly by the offset effect. It is noticed that although the regenerator has better regenerating and cooling effects with more diluted solution at the inlet, the solution inlet concentration is more of a non-controllable parameter since it is from dehumidifier directly. By contrast, the regenerator benefits from the high solution temperature owing to enhanced re-concentration and cooling effects. But the high solution outlet temperature means more cooling is needed before the solution enters the dehumidifier. Thus more follow up studies on optimization design for the whole system are required.

7.4. Effects of air properties

Compared with the solution inlet properties, the air inlet properties are easier to be controlled in practice. The influences of the inlet air temperature $T_{air,in}$ and humidity ratio $W_{air,in}$ on the regenerator effectiveness, TDR, MFR and $C_{sol,out}$ are analysed in this section. Variations of the effectiveness, TDR, MFR and $C_{sol,out}$ with $T_{air,in}$ under $W_{air,in} = 12\ g/kg\ dry\ air$ are shown in Figs. 18 and 19.

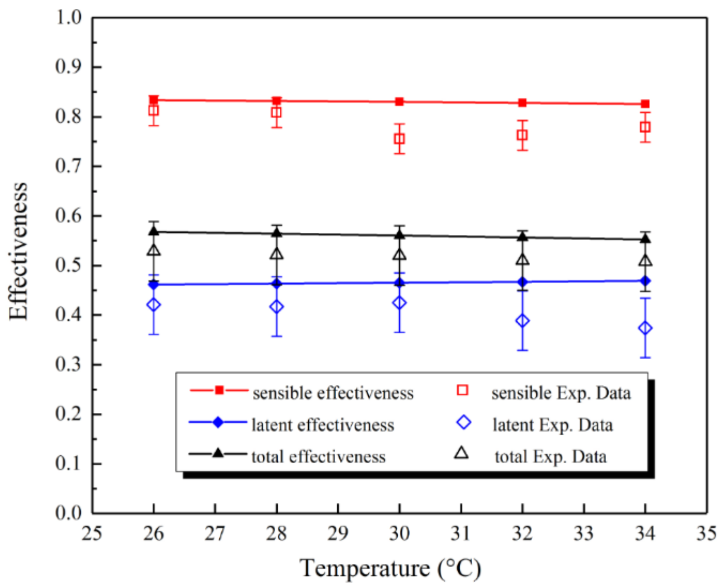

Fig. 18. Variations of effectiveness with $T_{air,in}$ under $W_{air,in} = 12\ g/kg\ dry\ air$

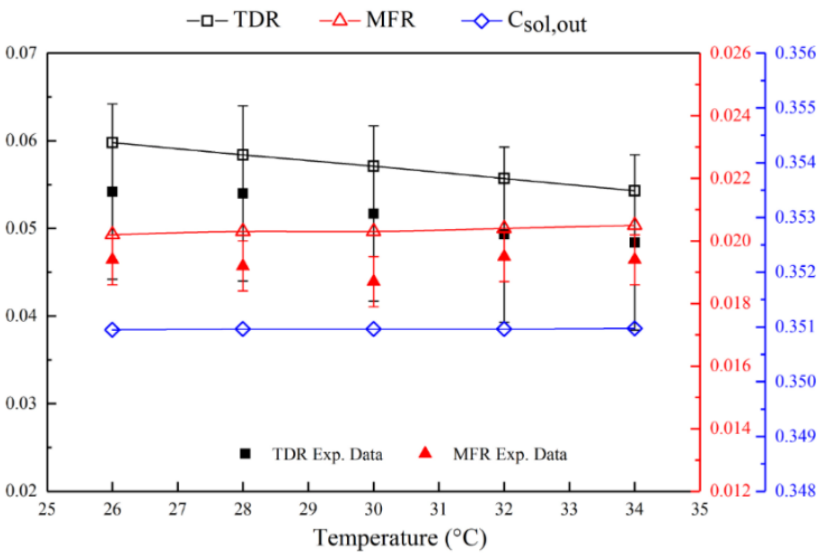

Fig. 19. Influences of $T_{air,in}$ on TDR, MFR and $C_{sol,out}$

Under the same $W_{air,in}$, the sensible effectiveness has the highest value, which is approximately twice of the latent effectiveness, while the total effectiveness is still in the middle as shown in Fig. 18. All effectiveness hardly vary with $T_{air,in}$ in the temperature range of 26°C to 34°C, and only change by 0.92%, 1.61% and 2.68% for the sensible, latent and total effectiveness respectively. For the latent heat transfer, air vapour pressure is only determined by air humidity ratio $W_{air,in}$ based on Eq. (32), and little impact on air vapour pressure would be imposed by changing air temperature only. Therefore, the mass transfer potential between the air and solution would remain constant in this case. Despite this, the latent effectiveness, MFR and $C_{sol,out}$ still increase slightly with $T_{air,in}$ as shown in Figs. 18 and 19. A possible explanation has been given in literature [29], the significant sensible heat transfer would occur between the air and solution when the solution temperature is higher than the air temperature. The cooling of the solution when contacting with the air would decrease the air vapour pressure, which restrains the regeneration. With higher temperature inlet air, there would be less sensible heat transfer from the solution to the air. Consequently, the vapour pressure difference between the air and solution sides can be maintained at a high level, and the latent heat transfer can still be enhanced slightly. On the other hand, the high $T_{air,in}$ would narrow the temperature difference between the air and solution, which deteriorates the sensible heat transfer potential. As a result, the sensible effectiveness and TDR are reduced to a small degree as illustrated in Figs. 18 and 19. Therefore, the effect of the air inlet temperature on the regeneration performance can be neglected, no obvious improvement can be achieved by adjusting $T_{air,in}$.

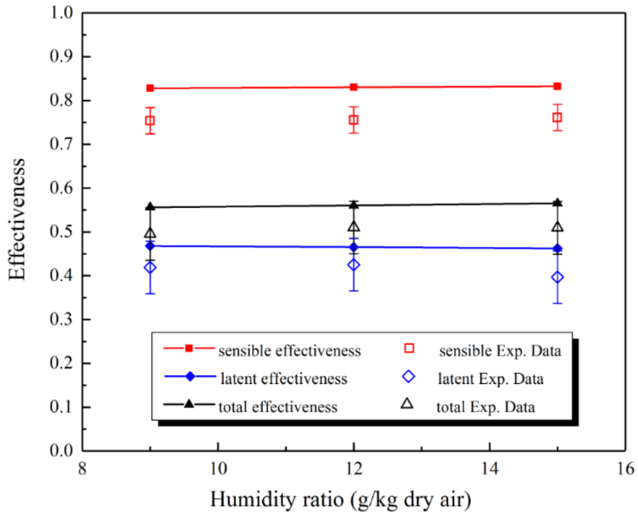

Fig. 20. Variations of effectiveness with $W_{air,in}$ under $T_{air,in} = 30℃$

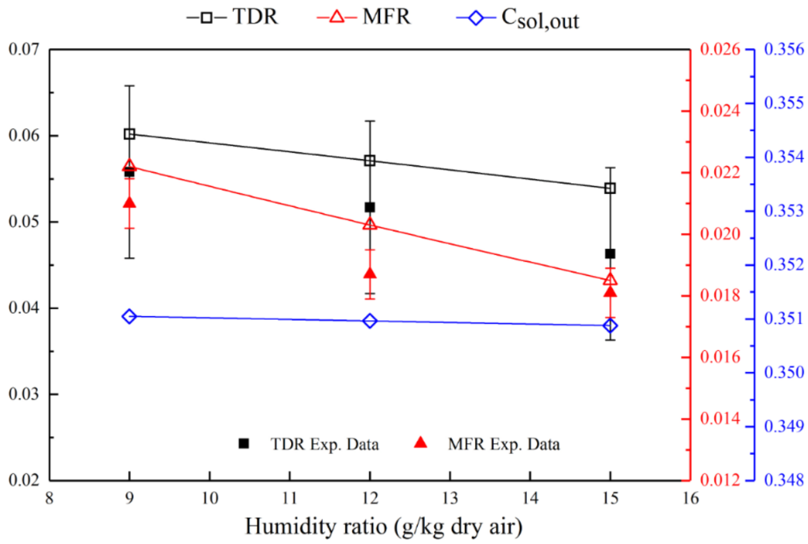

Fig. 21. Influences of $W_{air,in}$ on TDR, MFR and $C_{sol,out}$

Variations of the effectiveness, TDR, MFR and $C_{sol,out}$ with $W_{air,in}$ under $T_{air,in} = 30℃$ are shown in Figs. 20 and 21. Similar to all cases discussed previously, the sensible effectiveness has the highest value, followed by the latent and total effectiveness. Based on Eq. (32), the air vapour pressure increases with its humidity ratio. With the remarkable reduction of vapour pressure difference between the air and solution sides, the mass transfer potential is reduced significantly as well. As a result, MFR is decreased considerably as displayed in Fig. 21. This trend is in accordance with those in previous studies [29, 30]. Nevertheless, the latent effectiveness decreases significantly as well in the previous studies, this can be regarded as an effectiveness difference between the air and solution sides. As shown in Fig. 21, $C_{sol,out}$ decreases slightly with $W_{air,in}$. As the result solution outlet mass fraction $X_{sol,out}$ is increased. With refer to the definition of the solution side latent effectiveness as given in Eq. (35), both the numerator and denominator are reduced, and the combined effect causes the ignorable reduction of the latent effectiveness. Regarding the sensible heat transfer, it is slightly affected by reduced heat absorption during the evaporation process when the mass transfer is weakened. So the air outlet temperature $T_{sol,out}$ would increase to a small extent, which results in the decrease of TDR. Furthermore, according to the definition of the solution side sensible effectiveness in Eq. (39), the denominator would remain constant while both $T_{sol,out}$ and $X_{sol,out}$ are increased. Consequently, the sensible effectiveness is almost independent of $W_{air,in}$ as the result of the combined effect. To sum up, despite all effectiveness barely change with $W_{air,in}$, the regenerator moisture removal and cooling effects can still be improved by drier air.

8. Conclusions

The regeneration performance of a membrane-based parallel-plate heat and mass exchanger is investigated in this paper, heat and moisture transfer characteristics between the solution and air through membranes are studied by numerical simulation and experimental test. Solution side effectiveness, temperature decrease rate (TDR) and moisture flux rate (MFR) are applied to evaluate the regeneration performance. The influences of main parameters are assessed respectively, which include: number of heat transfer units (NTU), solution to air mass flow rate ratio (m^*), solution inlet temperature ($T_{sol,in}$), solution inlet concentration ($C_{sol,in}$), air inlet temperature ($T_{air,in}$) and humidity ratio ($W_{air,in}$). The conclusions can be drawn as follows:

- The boundary conditions of the membrane surface are neither uniform temperature nor uniform humidity ratio, and they change along the diagonal line of the membrane.
- NTU and m^* have the most significant effects on the regeneration performance, and their effects are interacted with each other. There is hardly benefit to the performance improvement by increasing NTU at low m^*(e.g. lower than 1). By contrast, no obvious performance enhancement is achieved by increasing m^* at low NTU (e.g. lower than 2).
- Although the regeneration performance can be improved by increasing NTU and m^*, their increasing gradients hardly change when NTU and m^* exceed NTU_{crit} and m^*_{crit}, which are 4 and 2 respectively in this study.
- Regenerator benefits from increased solution temperature as enhanced re-concentration (0.8% increase of MFR) and cooling effects (13.7% increase of TDR). However more cooling energy is required for the high temperature desiccant solution.
- Neither $T_{air,in}$ nor $W_{air,in}$ has remarkable influence on the regeneration performance, though the solution re-concentration ability can be enhanced slightly by applying drier and warmer air.

References

[1] Perez-Lombard L, Ortiz J, Pout C. A review on buildings energy consumption information, Energy and Buildings. 2008; 40:394－398.

[2] Ge GM, Xiao F, Niu XF. Control strategies for a liquid desiccant air-conditioning system, Energy and Buildings. 2011; 43:1499-1507.

[3] Das RS, Jain S. Performance characteristics of cross-flow membrane contractors for liquid desiccant systems, Applied Energy. 2015; 141:1-11.

[4] The CIBSE Journal CPD Programme: liquid desiccant for dehumidification in building air conditioning systems.

[5] T. Welch, in: H. Carwarardine, K. Butcher (Eds.), CIBSE Knowledge Series: KS13—Refrigeration, CIBSE Publications, London, UK, 2008.

[6] Dai YJ, Wang RZ, Zhang HF, Yu JD. Use of liquid cooling to improve the performance of vapor compression air conditioning, Applied Thermal Engineering. 2001; 21:1185-1202.

[7] Liu XH, Geng KC, Lin BR, Jiang Y. Combined cogeneration and liquid desiccant system applied in a demonstration building, Energy and Buildings. 2004; 36:945-953.

[8] Kinsara AA, Elsayed MM, Al-Rabghi OM. Proposed energy-efficient air conditioning system using liquid desiccant, Applied Thermal Engineering. 1996; 16(10):791-806.

[9] Huang SM, Zhang LZ. Researches and trends in membrane-based liquid air dehumidification, Renewable and Sustainable Energy Reviews. 2013; 28:425-440.

[10] Liu XH, Jiang Y, Yi XQ. Effect of regeneration mode on the performance of liquid desiccant packed bed regenerator, Renewable Energy. 2009; 34(1):209-16.

[11] Moghaddam DG, Oghabi A, Ge GM, Besant RW, Simonson CJ. Numerical model of a small-scale liquid-to-air membrane energy exchanger: Parametric study of membrane resistance and air side convective heat transfer coefficient, Applied Thermal Engineering. 2013; 61; 245-258.

[12] Moghaddam DG, Le Poudre P, Besant RW, Simonson CJ. Steady-state performance of a small-scale liquid-to-air membrane energy exchanger for different heat and mass transfer directions, and liquid desiccant types and concentrations: experimental and numerical data, ASMEJ Heat Transfer. 2013; 135:1–13.

[13] Moghaddam DG, LePoudre P, Ge GM et al. Small-scale single-panel liquid-to-air membrane energy exchanger (LAMEE) test facility development, commissioning and evaluating the steay-state performance, Energy and Buildings. 2013; 66:424-436.

[14] Bai HY, Zhu J, Chen ZW, Chu JZ. Parametric analysis of a cross-flow membrane-based parallel-plate liquid desiccant dehumidification system: numerical and experimental data, Energy and Buildings, 2018; 158:494-508.

[15] Zhang LZ. Heat and mass transfer in a cross-flow membrane-based enthalpy exchanger under naturally formed boundary conditions, International Journal of Heat and Mass Transfer. 2007; 50:151-162.

[16] Zhang LZ, Liang CH, Pei LX. Conjugate heat and mass transfer in membrane-formed channels in all entry regions, International Journal of Heat and Mass Transfer. 2010; 53:815-824.

[17] Huang SM, Zhang LZ, Tang K, Pei LX. Fluid flow and heat mass transfer in membrane parallel-plates channels used for liquid desiccant air dehumidification. International Journal of Heat and Mass Transfer 2012; 55:2571-2580.

[18] Huang SM, Zhang LZ, Yang ML. Conjugate heat and mass transfer in membrane parallel-plates ducts for liquid desiccant air dehumidification: Effects of the developing entrances. Journal of Membrane Science 2013; 437:82-89.

[19] Huang SM, Zhong ZR, Yang ML. Conjugate heat and mass transfer in an internally-cooled membrane-based liquid desiccant dehumidifier (IMLDD), Journal of Membrane Science. 2016; 508:73-83.

[20] Huang SM, Qiu D, Huang WH, Yang ML, Xiao HM. Laminar flow and heat transfer in a quasi-counter flow parallel-plate membrane channel in the solution side with cooling tubes, International Journal of Heat and Mass Transfer. 2017; 105:769-780.

[21] Qiu D, Wu ZH, Huang SM, Ye WB, Chen XL, Luo JC, Yang ML. Laminar flow and heat transfer in and internally-cooled hexagonal parallel-plate membrane channel (IHPMC), Applied Thermal Engineering. 2017; 124: 767-780.

[22] Labban O, Chen TY, Ghoniem AF, Lienhard V JH, Norford LK. Next-generation HVAC: Prospects for and limitations of desiccant and membrane-based dehumidification and cooling, Applied Energy. 2017; 200:330-346.

[23] Yang B, Yuan WX, Shang YH, Wang J, Wei B. Numerical and experimental study of a novel three-fluid membrane dehumidification method applied to spacecraft humidity control, Journal of Membrane Science. 2017; 530:112-124.

[24] Qi RH, Li DJ, Zhang LZ. Experimental investigation on membrane-based electrolytic dehumidification for air-conditioning systems, Procedia Engineering. 2017; 205:3194-3198.

[25] Fumo N, Goswami DY. Study of an aqueous lithium chloride desiccant system: air dehumidification and desiccant regeneration, Solar Energy. 2002; 72(4):351-61.

[26] Longo GA, Gasparella A. Experimental analysis on desiccant regeneration in a packed column with structured and random packing, Solar Energy. 2009; 83(4):511-21.

[27] Liu XH, Jiang Y, Chang XM, Yi XQ. Experimental investigations of the heat and mass transfer between air and liquid desiccant in a cross-flow regenerator, Renewable Energy. 2007; 32:1623-1636.

[28] Li XW, Zhang XS, Quan S. Single-stage and double-stage photovoltaic driven regeneration for liquid desiccant cooling system, Applied Energy. 2011; 88:4908-4917.

[29] Yang ZL, Zhang KS, Hwang YH, Lian ZW. Performance investigation on the ultrasonic atomization liquid desiccant regeneration system, Applied Energy. 2016; 171:12-25.

[30] Ge GM, Moghaddam DG, Abdel-Salam AH, Besant RW, Simonson CJ. Comparison of experimental data and a model for heat and mass transfer performance of a liquid-to-air membrane energy exchanger (LAMEE) when used for air dehumidification and salt solution regeneration, International Journal of Heat and Mass Transfer. 2014; 68:119-131.

[31] Moghaddam DG, Besant RW, Simonson CJ. Solution-side effectiveness for a liquid-to-air membrane energy exchanger used as a dehumidifier/regenerator, Applied Energy. 2014; 113:872-882.

[32] Mander P (2012) How to convert relative humidity to absolute humidity available at <https://carnotcycle.wordpress.com/2012/08/04/ how-to-convert-relative-humidity-to-absolute-humidity/>.

[33] ASHRAE, *2013 ASHRAE Handbook Fundamentals.* Atlantal 2013.

[34] Cisternas LA and Lam EJ. An analytic correlation for the vapour pressure of aqueous and non-aqueous solutions of single and mixed electrolytes. Part II. Application and extension, Fluid Phase Equilib. 1991; 62:11-27.

[35] ANSI/ASHRAE STANDARD 84-2013, Method of test for air-to-air heat/energy exchangers, American society of heating, refrigerating, and air-conditioning engineers, Atlanta.

[36] Yang ZL, Lin BB, Zhang KS, Lian ZW. Experimental study on mass transfer performance of the ultrasonic atomization liquid desiccant dehumidification system, Energy and Buildings. 2015; 93:126-136.

[37] Chen ZW, Zhu J, Bai HY. Performance assessment of a membrane liquid desiccant dehumidification cooling system based on experimental investigations, Energy and Buildings. 2017; 139:665-679.

[38] Chen ZW, Zhu J, Bai HY, Yan YY, Zhang LL. Experimental study of a membrane-based dehumidification cooling system, Applied Thermal Engineering. 2017; 115:1315-1321.

[39] Taylor JR. An Introduction to Error Analysis: The Study of Uncertainties in Physical Measurements, second ed., University Science Books, Sausalito, CA, 1997.

[40] Niu JL, Zhang LZ. Membrane-based enthalpy exchanger: material considerations and clarification of moisture resistance, Journal of Membrane Science. 2001; 189(2):179-191.

[41] Namvar R, Pyra D, Ge GM, Simonson CJ. Transient characteristics of a liquid-to-air membrane energy exchanger (LAMEE) experimental data with correlations, International Journal of Heat and Mass Transfer. 2012; 55:6682-6694.